

Asymmetric Rayleigh-Taylor and double-diffusive fingers in reactive systems

L. Lemaigre, M. A. Budroni, L. A. Riolfo, P. Grosfils, and A. De Wit

Citation: *Phys. Fluids* **25**, 014103 (2013); doi: 10.1063/1.4774321

View online: <http://dx.doi.org/10.1063/1.4774321>

View Table of Contents: <http://pof.aip.org/resource/1/PHFLE6/v25/i1>

Published by the [American Institute of Physics](#).

Related Articles

Influence of a simple magnetic bar on buoyancy-driven fingering of traveling autocatalytic reaction fronts
[Phys. Fluids 24, 124101 \(2012\)](#)

The effect of rotation on the Rayleigh-Bénard stability threshold
[Phys. Fluids 24, 114101 \(2012\)](#)

Variable viscosity effects on the dissipation instability in a porous layer with horizontal throughflow
[Phys. Fluids 24, 104102 \(2012\)](#)

Proper orthogonal decomposition investigation of turbulent Rayleigh-Bénard convection in a rectangular cavity
[Phys. Fluids 24, 105106 \(2012\)](#)

Flow states in two-dimensional Rayleigh-Bénard convection as a function of aspect-ratio and Rayleigh number
[Phys. Fluids 24, 085104 \(2012\)](#)

Additional information on Phys. Fluids

Journal Homepage: <http://pof.aip.org/>

Journal Information: http://pof.aip.org/about/about_the_journal

Top downloads: http://pof.aip.org/features/most_downloaded

Information for Authors: <http://pof.aip.org/authors>

ADVERTISEMENT



**Running in Circles Looking
for the Best Science Job?**

Search hundreds of exciting
new jobs each month!

<http://careers.physicstoday.org/jobs>

physicstodayJOBS



Asymmetric Rayleigh-Taylor and double-diffusive fingers in reactive systems

L. Lemaigre,^{1,a)} M. A. Budroni,^{1,a)} L. A. Riolfo,¹ P. Grosfils,² and A. De Wit^{1,2}

¹*Nonlinear Physical Chemistry Unit, Faculté des Sciences, Université Libre de Bruxelles (ULB), CP231, 1050 Brussels, Belgium*

²*Center for Nonlinear Phenomena and Complex Systems, Université Libre de Bruxelles (ULB), CP231, 1050 Brussels, Belgium*

(Received 8 August 2012; accepted 20 December 2012; published online 25 January 2013)

Buoyancy-driven flows induced by the hydrodynamic Rayleigh-Taylor or double-diffusive instabilities develop symmetrically around the initial contact line when two solutions of given solutes with different densities are put in contact in the gravitational field. If the solutes affecting the densities of these solutions are involved in chemical reactions, changes in composition due to the underlying reaction-diffusion processes can modify the density profile in space and time, and affect the hydrodynamic patterns. In particular, if the density difference between the two reactant solutions is not too large, the resulting chemo-hydrodynamic patterns are asymmetric with regard to the initial contact line. We quantify both experimentally and numerically this asymmetry showing that fingers here preferentially develop above the reaction zone and not across the mixing zone as in the non reactive situation. In some cases, the reaction can even lead to the onset of a secondary double-diffusive instability between the product of the reaction, dynamically generated *in situ*, and one of the reactants. © 2013 American Institute of Physics. [<http://dx.doi.org/10.1063/1.4774321>]

I. INTRODUCTION

Buoyancy-driven instabilities in fluids are genuine sources of fluid motions.^{1,2} The well-known Rayleigh-Taylor (RT) instability occurs as soon as a denser solution overlies a less dense one in the gravitational field^{1,3} like typically when salted water sinks into fresh water. This instability has been the subject of numerous studies as it impacts several climatic, environmental, and industrial applications. The double-diffusive (DD) instability is another buoyancy-driven instability,^{4,5} which arises when two different contributions to the density profile are opposing (classically heat and mass, but it can also be that of two different solutes^{2,6,7}). DD occurs when the total density profile is stable (i.e., density increases downwards along the gravitational field) but the destabilizing component (heat, for instance) diffuses faster than the stabilizing one (mass). It leads to convective motions that have been well studied in oceanography⁸ (where it leads to so-called “salt fingers”), geology,⁹ or in the analysis of convection in star or planet mantles,⁵ for instance.

In some applications like industrial processes,¹⁰ CO₂ storage,¹¹ or thermonuclear burning of stars,¹² for instance, such convective motions may interplay with chemical reactions. The coupling arises when the reaction dynamically modifies a physical property of the flow like its density, viscosity, or surface tension.^{13,14} This change in turn can affect the flows but in some cases can also more drastically modify the patterns or even trigger an instability in an otherwise stable system.¹⁵

In the case of buoyancy-driven instabilities, such a chemo-hydrodynamic coupling has already been well studied for traveling autocatalytic fronts (see Refs. 16–18 and references therein) and combustion problems.^{12,19} In parallel, the coupling between convective motions and a simple $A + B \rightarrow C$ reaction has been addressed both experimentally^{20–29} and theoretically.^{24,27,29–32} In the specific

^{a)}L. Lemaigre and M. A. Budroni contributed equally to this work.

case of acid-base reactions, buoyancy-driven destabilization of the miscible interface between two solutions containing the separate reactants A and B has been studied in Hele-Shaw cells (two glass plates separated by a thin gap and oriented vertically in the gravitational field). In horizontal systems, convection within the gap is characterized by one or two convection rolls^{29–31} that affect the propagation speed of the underlying $A + B \rightarrow C$ reaction-diffusion front.³³ In vertical systems, if an aqueous solution of HCl is put on top of a denser aqueous solution of NaOH, convective motions rapidly develop above the miscible contact line.^{24,27} These are due to a diffusive layer convection (DLC) mechanism^{2,34} arising when a less dense solution of a fast diffusing component overlies a denser solution of a slow diffusing one. As the acid diffuses faster than the base, a depletion zone is created dynamically in time above the contact line where the acid has diffused out without being replaced yet by the slow diffusing base. Another pattern sometimes also appears below the contact line but with a different wavelength.^{22,26} These lower structures have however been attributed to the presence of the color indicator used to visualize the convective patterns and acting as an effective reactant modifying the density profile.^{25,26} In absence of a color indicator, visualization can be made by interferometry²⁴ or schlieren techniques.²⁷ In that case, the DLC convective plumes are observed only *above* the contact line. This is different from the non reactive situation³⁴ where convection is also obtained below the miscible interface where the fast diffusing species is accumulating. The asymmetry of the DLC pattern is related to the chemical reaction which consumes the acid before it can accumulate in the lower layer and replaces it by a third species of intermediate contribution to density. These experiments clearly show that the chemical reaction affects the symmetry of the DLC pattern.

In this context, it is of interest to understand to what extent such an active role of chemistry can affect RT or DD patterns as well. Indeed, RT and DD modes are encountered in numerous systems, and it is therefore important to know whether the properties of RT and DD patterns are the same or not in reactive systems. Some theoretical works have already demonstrated that reactions can affect the stability properties of DD modes,^{35–37} however, their active influence on nonlinear dynamics remains largely unexplored.

To do so, we study here by combined experimental and theoretical analysis, the influence of a simple $A + B \rightarrow C$ chemical reaction on buoyancy-driven Rayleigh-Taylor and double diffusion instabilities. We consider a stratification of a solution of reactant A on top of a miscible solution of reactant B within a Hele-Shaw cell oriented vertically in the gravitational field. In absence of reaction, a RT instability is obtained if the density ρ_A of the upper solution is larger than the density ρ_B of the lower one. If we start from an initially statically stable configuration ($\rho_A < \rho_B$), DD modes are obtained if B diffuses sufficiently faster than A.^{2,4,6} If A reacts with B to yield the product C, then the density profile is affected in space and time by the reaction.

We demonstrate that, in that case, the reaction can have a profound influence on the dynamics as it breaks the symmetry of the RT and DD patterns. Indeed, instead of deforming the miscible interface symmetrically around the position of the initial contact line, the convective structures develop only above it. In some cases, a second structure appears later in time and can be attributed to the dynamic generation of the product C in the course of time. We analyze the changes in patterns by comparing experiments done using non reactive solutions and reactive acid-base systems. We quantitatively compute the amplitude of the symmetry breaking as a function of the relative concentrations of the two reactants A and B. We enlighten the experimental results by numerical simulations of a reaction-diffusion-convection (RDC) model of buoyancy-driven convection triggered around an $A + B \rightarrow C$ reaction-diffusion front using values of parameters dictated by the experiments. Good agreement between both experimental and numerical results is obtained.

This article is organized as follows: Section II describes the experimental results, while the theoretical study is presented in Sec. III before conclusions are addressed in Sec. IV.

II. EXPERIMENTAL STUDY

Let us first describe the experimental set-up and the chemicals used before reviewing the properties of the hydrodynamic patterns obtained experimentally with and without reactions.

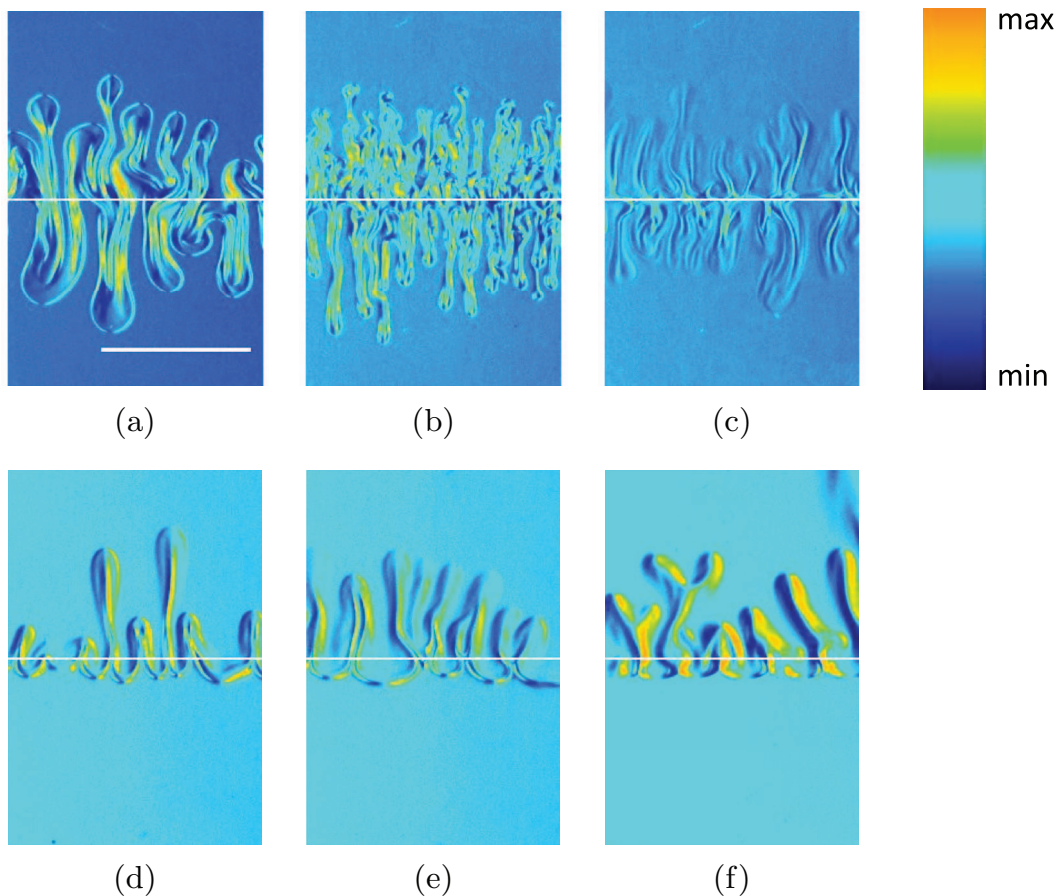


FIG. 1. Refractive index modulations of the experimental non reactive (top) and reactive (bottom) buoyancy-driven patterns: (a) non reactive Rayleigh-Taylor, (b) non reactive double diffusion, (c) non reactive diffusive layer convection, (d) reactive Rayleigh-Taylor, (e) reactive double diffusion, and (f) reactive diffusive layer convection. Time of the snapshots: (a) 5 s, (b) 18 s, (c) 68 s, (d) 15 s, (e) 30 s, and (f) 151 s. The field of view of each image is $1.8 \text{ cm} \times 2.7 \text{ cm}$. The scale bar represents a length of 1 cm. The horizontal middle line is added to show the position of the initial contact line.

A. Experimental set-up

The experimental set-up consists in a Hele-Shaw cell made of two borosilicate glass plates separated by a thin polymer spacer giving a gap width of 0.5 mm. Specific injection holes and exhaust system allow to obtain a well-defined planar interface between two miscible solutions within the gravitational field.³⁸ To avoid the perturbative influence of any color indicator on the dynamics,^{25,26} we use the aqueous solutions as prepared, and, as they are transparent, a phase-shifting schlieren technique is used to track the convective patterns.^{39,40} This optical technique allows to visualize the variations in space and time of the refractive index, which can in turn be related to the density variations inside the solutions. The images show the refractive index gradients in a grey scale but a colormap has been added here to enhance the contrast. This colormap is presented in Fig. 1 and is the same for all experimental figures. The largest values of this map correspond to sharp gradients of refractive index and indicate strong density variations. Changes in brightness from one picture to the other are related to the acquisition process of the pictures. All experimental figures have a field of view of $1.8 \text{ cm} \times 2.7 \text{ cm}$. Aqueous solutions of NaCl and sucrose in various compositions are chosen to analyze non reactive hydrodynamic instabilities, while aqueous solutions of NaOH and HCl are used to study the same instabilities in presence of a chemical reaction. A summary of the composition and the related densities of the various solutions are given in Table I.

TABLE I. Concentrations and densities of the different solutions used during the experiments. Solutions were prepared with sucrose Sigma BioUltra $\geq 99.5\%$, NaCl Sigma Ultra $\geq 99.5\%$, NaOH Chem Lab for analysis 99%, and 6 mol/l HCl Fluka analytical volumetric solutions. The density is measured at the temperature of the sample given in column 4.

Solute	Concentration (± 0.004 mol/l)	Density (± 0.0005 g/cm ³)	Temperature (± 0.1 °C)
Sucrose	0.500	1.0651	23.0
NaCl	0.300	1.0119	23.8
NaCl	0.683	1.0280	23.4
NaCl	1.456	1.0597	23.4
NaCl	1.715	1.0673	23.2
NaOH	0.200	1.0084	22.7
NaOH	0.300	1.0125	23.5
NaOH	0.400	1.0167	23.5
NaOH	0.500	1.0208	23.6
NaOH	0.600	1.0253	23.5
NaOH	0.700	1.0291	23.6
NaOH	0.800	1.0331	23.7
NaOH	0.900	1.0370	24.5
NaOH	1.000	1.0408	24.2
HCl	1.000	1.0171	22.9

B. Non reactive buoyancy-driven patterns

Let us first remind the classical RT, DD, and DLC dynamics that develop in the absence of any chemical reaction when two miscible solutions containing solutes A and B of different densities are put in contact in a vertical Hele-Shaw cell (see top of Fig. 1). Figure 1(a) shows refractive index changes for the Rayleigh-Taylor instability obtained by putting a denser solution of NaCl in concentration 0.683 mol/l on top of pure water. Vivid convection is obtained immediately after contact and leads to convective fingers extending both upwards and downwards, and deforming the initial contact line keeping an up-down symmetric mixing zone. Indeed, on average, the fingers extend on the same distance above and below the initial position of the interface.

In order to trigger double diffusion, a solution of sucrose in concentration 0.5 mol/l and density 1.0651 g/cm³ is put on top of a denser solution of NaCl in concentration 1.715 mol/l and of density 1.0673 g/cm³ (Fig. 1(b)). As the salt NaCl diffuses roughly three times faster than sucrose ($D_{NaCl} = 1.611 \times 10^{-5}$ cm²/s,⁴¹ while $D_{sucrose} = 0.523 \times 10^{-5}$ cm²/s⁴²), the denser stabilizing component B on the bottom diffuses thus faster than the stabilizing component A on top within an initially statically stable situation. These provide the conditions for a DD instability also deforming the interface into rising and sinking fingers extending symmetrically around the initial contact line (Fig. 1(b)). Note that more time is needed to reach a same mixing zone than in the RT case, as diffusion (which is a slow process) has to act to destabilize the system.

The third possible buoyancy-driven instability is the DLC one obtained when starting from a stable density gradient but with the upper component A diffusing faster than the lower component B. Putting a less dense solution of salt (in concentration 1.456 mol/l and of density 1.0597 g/cm³) on top of the denser 0.5 mol/l solution of sucrose produces the DLC convective patterns seen in Fig. 1(c). As already observed experimentally³⁴ and discussed theoretically,² DLC modes develop convection cells both above and below the contact line, which remains unperturbed at early times. These fluid motions appear at the locations where the depletion and accumulation zones develop due to the fact that component A diffuses faster towards the lower layer than the component B diffuses upwards.² Appreciate that more than a minute is necessary for the DLC fingers to extend on a same distance as that reached by RT modes in 5 s. The DLC mechanism needs indeed more time for diffusion to trigger the adverse local density gradients at the origin of the convection.

To sum up, as soon as non reactive solutions containing various solutes are put in contact in the gravitational field, convective modes develop because of either RT, DD, or DLC mechanisms. In

all three cases, convective patterns develop symmetrically around the initial contact line. The only stable configuration is the one for which $\rho_A < \rho_B$ and $D_A \sim D_B$.²

C. Reactive convective patterns

Let us now focus on the corresponding reactive cases (see bottom of Fig. 1) obtained when A and B are involved into a reaction. The dynamics were studied in the particular case of the acid-base reaction between HCl and NaOH. Their respective diffusion coefficients are $D_{HCl} = 3.336 \times 10^{-5} \text{ cm}^2/\text{s}$ ⁴¹ and $D_{NaOH} = 2.129 \times 10^{-5} \text{ cm}^2/\text{s}$.⁴¹ As $D_{HCl} > D_{NaOH}$, reactive DLC is obtained when starting from a less dense solution of HCl on top of a denser solution of NaOH. Figure 1(f) shows an example for 1 mol/l HCl ($\rho = 1.0171 \text{ g/cm}^3$) on top of 0.5 mol/l NaOH ($\rho = 1.0208 \text{ g/cm}^3$). Reactive DLC has already been extensively studied both without^{24,27} and with^{22,25,26} color indicator, and will not be further addressed here. We recall however that, in this case, the reactive DLC patterns are asymmetric with regard to the contact line^{24,27} as seen in Fig. 1(f).

Let us focus on both RT and DD cases. Both can be obtained when a solution of NaOH is put on top of a solution of the faster diffusing acid. We will, in the remainder of the article, keep the lower HCl concentration fixed to 1 mol/l ($\rho = 1.0171 \text{ g/cm}^3$) and vary the concentration of the upper NaOH solution. If the top solution is less or equally dense ($\rho_{NaOH} \leq 1.0171 \text{ g/cm}^3$), then DD convection develops as the faster diffusing acid is in the lower layer (see Fig. 1(e) for NaOH 0.4 mol/l and $\rho = 1.0167 \text{ g/cm}^3$). The development of the convective fingers during time is shown on Fig. 2. RT is

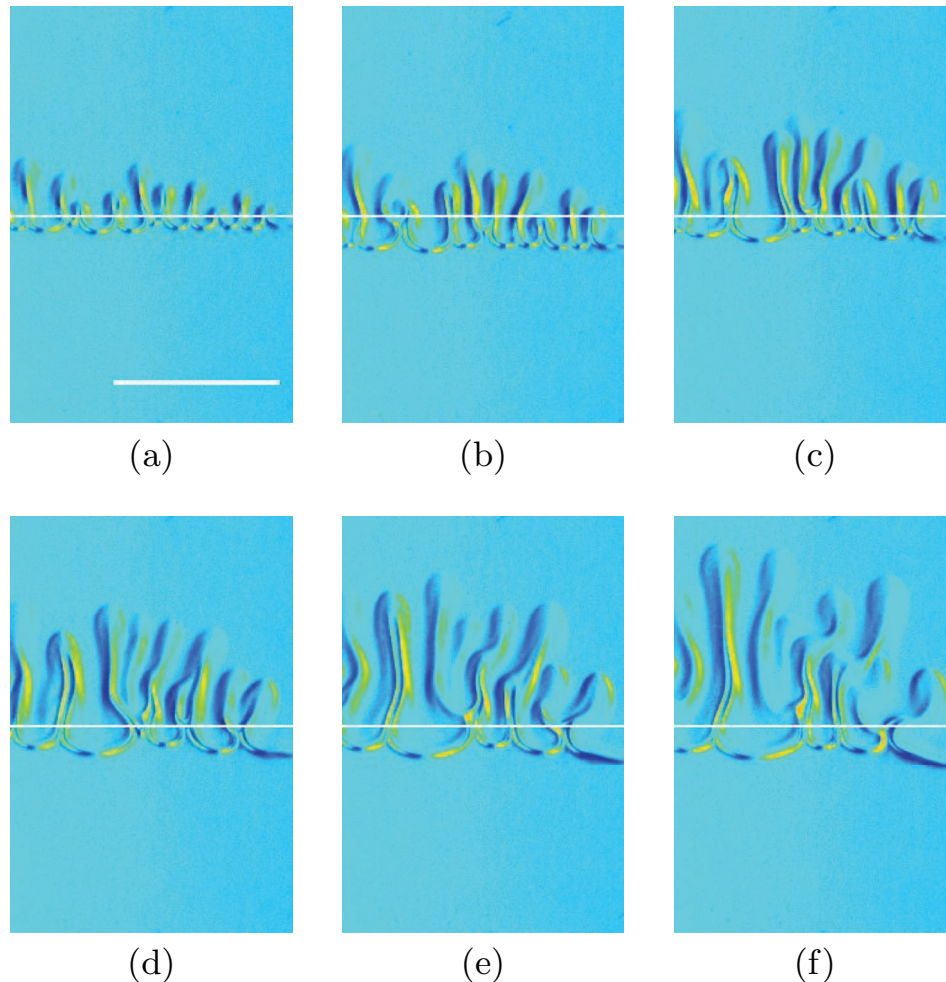


FIG. 2. Evolution in time of the reactive DD convective patterns obtained with NaOH 0.4 mol/l on top of HCl 1 mol/l. Time of the snapshots: (a) 15 s, (b) 20 s, (c) 25 s, (d) 30 s, (e) 35 s, and (f) 40 s. The scale bar represents a length of 1 cm.

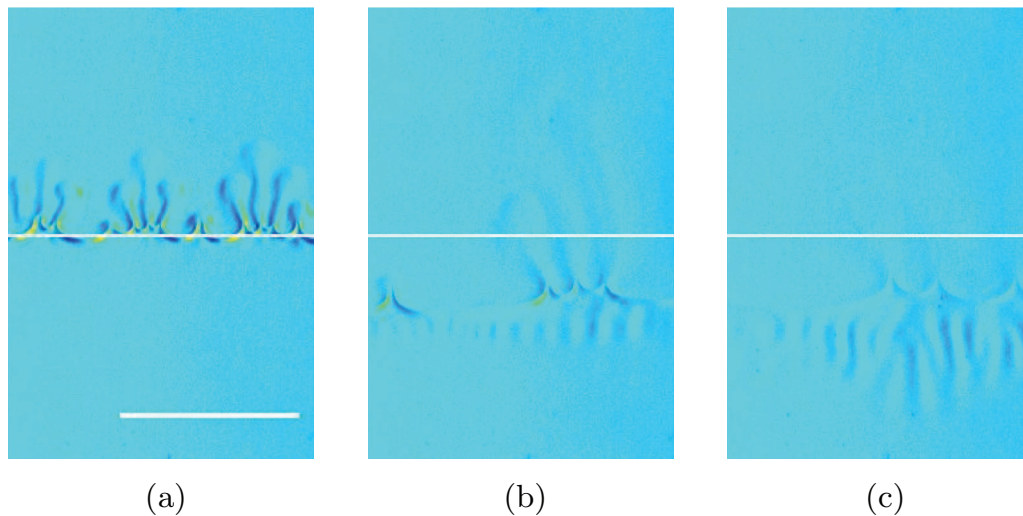


FIG. 3. Reactive convective patterns obtained when a solution of NaOH 0.3 mol/l is put on top of a 1 mol/l HCl solution. Time of the snapshots: (a) 30 s, (b) 15 min, and (c) 32 min 30 s. The scale bar represents a length of 1 cm.

obtained for denser NaOH on top (see Fig. 1(d) with NaOH 0.5 mol/l and $\rho = 1.0208 \text{ g/cm}^3$). Even though DD and RT fingers look very similar, they can readily be differentiated experimentally thanks to the initial condition (RT if the upper solution is denser than the lower one and DD in the reverse case) and the time scales on which they evolve. As seen in Fig. 6, less than 3 s are needed for RT fingers to grow half a centimeter and very vigorous convection is observed while 10–50 s are needed for onset of the milder convection in DD.

As can be seen by comparing the top and bottom rows of Fig. 1, the chemical reaction breaks the symmetry of the convective patterns. Indeed, instead of developing fingers both above and below the initial contact line, the fingers grow in the reactive case preferentially above this line. This observation is particularly surprising for the Rayleigh-Taylor instability, where the vivid convective flows due to the unfavorable difference in densities are usually expected to slave any chemistry. As shown in Sec. II D, this breaking of symmetry only operates if the density difference $\Delta\rho$ between the two solutions is small enough to be dynamically affected by the reaction. Above a given $\Delta\rho$, the reaction is not efficient enough to have an impact and the classical symmetric Rayleigh-Taylor convective modes take over again.

Besides the breaking of symmetry, the reactive system also shows the possibility of coexistence within the same system of two different patterns originating from successive instabilities. An example is shown in Fig. 3. As we start from a less dense 0.3 mol/l solution of NaOH on top of HCl, an asymmetric DD pattern appears at early time. Much later on, another pattern appears in the lower layer in the shape of thin vertical stripes, which elongate downwards and deform during time. The occurrence of this secondary pattern is due to a double-diffusive instability between the NaCl, dynamically produced in the reaction zone, and the underlying HCl. To prove this, we have checked that similar fingers develop within a few minutes in absence of any reaction when a solution of NaCl in concentration 0.3 mol/l is put on top of a denser 1 mol/l solution of HCl inside a Hele-Shaw cell (Fig. 4). In the reactive case (Fig. 3), the analogous DD pattern takes however much longer (~ 15 min) to appear as a secondary instability resulting from the reaction between NaOH and HCl because it requires the reaction to generate enough NaCl product in the middle reaction zone for DD between NaCl above HCl to develop.

D. Influence of the concentrations

In order to study the influence of changes in the concentration on the dynamics, the concentration of the top solution (NaOH) is varied while keeping the concentration of the bottom solution (HCl)

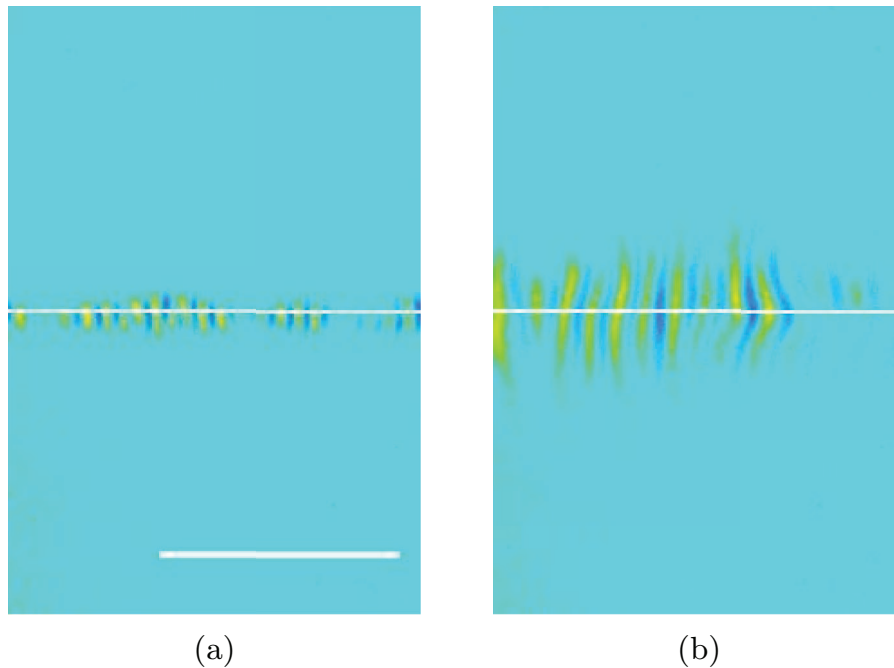


FIG. 4. Non reactive double-diffusive pattern obtained with a solution of NaCl 0.3 mol/l on top of HCl 1 mol/l. Time of the snapshots: (a) 53 s and (b) 124 s. The scale bar represents a length of 1 cm.

to 1 mol/l and the related density to 1.0171 g/cm^3 . The vertical extension of the patterns is measured by image processing to quantify the growth of the patterns. First, the experimental pictures of the refractive index are binarized and the noise is removed with a MATLAB program. The binarized pictures display white convective patterns on a black background. By summing the values of the pixels along a horizontal line, we obtain a vector of the size of the length of the picture that has elements equal to zero if their index corresponds to a row with only black pixels and to a non zero value otherwise. Non zero elements of this vector thus represent the convective zone and their index gives us the position of this convective zone in the experimental picture. The first and the last non zero elements provide the top location z_{top} and the bottom z_{bottom} one of the convective zone. Knowing the position z_0 of the initial contact line with regard to $z = 0$ at the lower side of the image, we can next define the upward and downward contribution to the length of the patterns: $L_m^+ = z_{top} - z_0$ and $L_m^- = z_{bottom} - z_0$. The lengths obtained for four experiments are averaged. These averaged lengths are plotted in Fig. 5 with L_m^+ corresponding to the extent of the upward growing mixing zone, and hence, to the curves with positive values, while L_m^- are those for the downward motions and negative values. It can be appreciated that these quantities have similar values at large NaOH concentrations, while $L_m^+ > |L_m^-|$ at lower concentrations (which is the sign of an asymmetry such that fingers extend more upwards than downwards). The total length of the mixing zone is then defined as $L_m = z_{top} - z_{bottom}$ and is shown in Fig. 6.

The cases of reactive double diffusion and Rayleigh-Taylor convection are hereafter commented separately. As can be seen from the densities in Table I, reactive double-diffusive cases are those for screened concentrations of the base up to 0.4 M ($\rho_A \leq \rho_B$), while reactive Rayleigh-Taylor occurs in our screened concentrations from 0.5 M on ($\rho_A > \rho_B$).

1. Double diffusion

As shown in Fig. 5(a), the upward contribution L_m^+ to the length of the DD fingers obtained when $\rho_A \leq \rho_B$ is clearly more important than the downward contribution L_m^- at lower concentrations in NaOH. Indeed, in that case, there are no fingers growing downwards. If we now consider the total length of the convective zone (Fig. 6), the growth of the fingers first presents an induction period

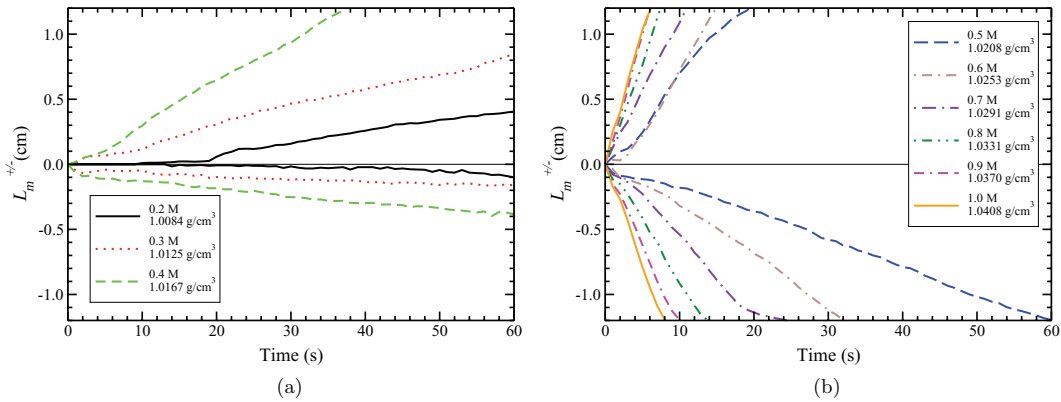


FIG. 5. Evolution of the upper ($L_m^+ \geq 0$) and lower ($L_m^- \leq 0$) extent of the fingers for different concentrations (and related densities) of the base solution. (a) Reactive double diffusion cases for which the density of the base solution is lower than or equal to 1.0171 g/cm^3 , the density of the 1 mol/l acid solution; (b) reactive Rayleigh-Taylor cases for NaOH densities larger than 1.0171 g/cm^3 . The continuous line at $L_m^\pm = 0$ represents the position of the initial contact line.

during which the length remains constant or increases very slowly. The induction time becomes shorter, i.e., convection takes in faster when the concentration of the alkaline solution increases. Moreover, once the growth has started, the curves are steeper, i.e., the pattern grows faster at larger concentrations.

2. Rayleigh-Taylor

In Fig. 5(b), it can be seen that, in the RT case, an asymmetry is clearly visible for NaOH concentrations lower than 0.9 M, but the convective zone develops more symmetrically around the initial contact line as the concentration of the top solution increases. The increase of the downward contribution is not only due to the downward movement of the reaction zone. Indeed, this base line gradually deforms and takes the shape of sinking fingers when the concentration is increased. At high alkaline concentrations, the sinking fingers develop as fast as the rising ones and a classical symmetric RT instability similar to that shown in Fig. 1(a) is recovered. Moreover, as the NaOH concentration increases, the density ratio also becomes larger and the system becomes more unstable. Hence, the induction time becomes shorter and the slope of the mixing length increases (Fig. 6).

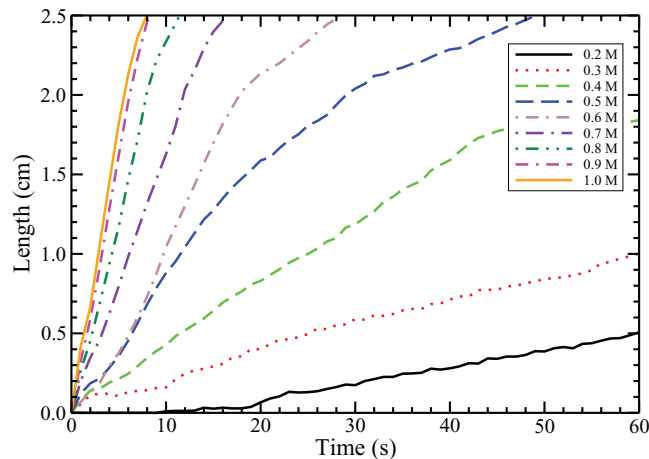


FIG. 6. Evolution of the length of the fingers for different concentrations of the NaOH solution. Densities for the related concentrations are given in Fig. 5.

III. THEORETICAL STUDY

In order to enlighten the experimental findings, let us now turn to numerical simulations of the corresponding reaction-diffusion-convection model.

A. Model

The Hele–Shaw cell is approximated by a two-dimensional vertical slab of width L_X and height L_Z in a (X, Z) reference frame, where the gravitational acceleration $\bar{g} = (0, -g)$ is oriented downwards along the Z axis. As sketched in Fig. 7 (left panel), the alkaline solution A, containing NaOH in the initial concentration A_0 and of density ρ_a^0 is placed on top of the HCl solution B, with concentration B_0 and density ρ_B^0 . The chemical reaction $A + B \rightarrow C$ (where C is the resulting salt NaCl) occurs between the two miscible solutions, which are initially sharply separated by a horizontal planar interface at $L_Z/2$. Although this reaction is well known to be exothermic, we apply the isothermal hypothesis to our model since, as heat diffuses much faster than mass, its contribution to the density gradients is quantitatively negligible.²⁷ According to the experimental data in Sec. II, the solutions are sufficiently diluted that the coefficients D_A , D_B , and D_C can be considered as constant and cross-diffusive terms neglected. Moreover, we can also assume a linear dependence of the density ρ upon the reactant concentrations:

$$\rho(A, B, C) = \rho_0 (1 + \alpha_A A + \alpha_B B + \alpha_C C), \quad (1)$$

where ρ_0 is the reference density of the solvent (water), and $\alpha_I = \frac{1}{\rho_0} \frac{\partial \rho}{\partial I}$ is the solutal expansion coefficient of solute I and I its concentration. Equation (1) relies on the assumption that all compounds diffuse as ionic pairs.²⁶

The spatio-temporal dynamics of the system obeys a set of partial differential equations in which the chemical kinetics of an $A + B \rightarrow C$ reaction, governed by the kinetic constant k , is coupled to Fickian diffusion and to natural convection described by the Stokes equations through the state equation (1). The dimensional form of the resulting reaction-diffusion-convection system is

$$\partial_t A + (\mathbf{V} \cdot \nabla) A = D_A \nabla^2 A - kAB, \quad (2)$$

$$\partial_t B + (\mathbf{V} \cdot \nabla) B = D_B \nabla^2 B - kAB, \quad (3)$$

$$\partial_t C + (\mathbf{V} \cdot \nabla) C = D_C \nabla^2 C + kAB, \quad (4)$$

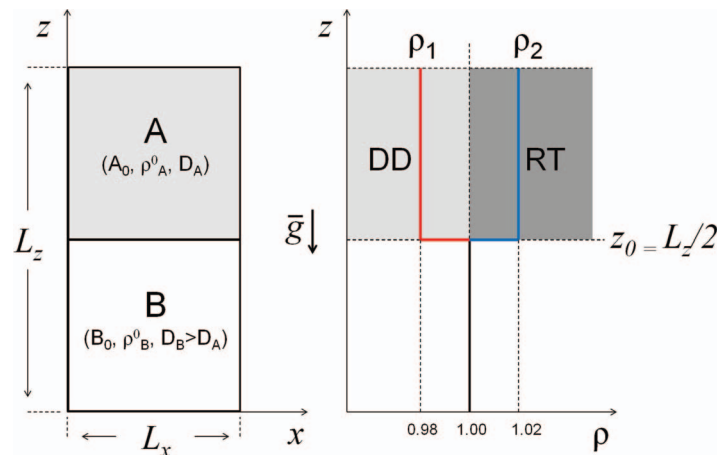


FIG. 7. (Left panel) Sketch of the vertical slab defining the spatial domain of our RDC problem. (Right panel) Two different initial density profiles for the nonlinear simulations. The density of the bottom solution is equal to 1 (black branch). The top solution density is varied by changing the initial concentration A_0 . The left branch ($\rho_1 = 0.98$, red online) gives a double-diffusive instability, while the right profile ($\rho_2 = 1.02$, blue online) leads to a Rayleigh-Taylor instability.

$$\nabla P = \mu \nabla^2 \mathbf{V} - \rho(A, B, C)g \mathbf{1}_z, \quad (5)$$

$$\nabla \cdot \mathbf{V} = 0. \quad (6)$$

Hydrodynamic equations are derived in the Boussinesq approximation,¹ assuming that density changes only affect the gravitational term ρg of Eq. (5). $\mathbf{V} = (U, V)^T$ is the velocity field, μ is the dynamic viscosity, and P is the pressure. The model is conveniently cast into a dimensionless form by using the time scale of the chemical process $t_c = 1/(kB_0)$, the reaction–diffusion characteristic length $L_c = \sqrt{D_B t_c}$, the velocity scale $V_c = L_c/t_c = \sqrt{D_B/t_c}$, while we use $P_c = \frac{\mu}{t_c}$ and B_0 , respectively, as the pressure and concentration scales.

Moreover, we define a dimensionless pressure gradient by including the hydrostatic pressure gradient term as $\nabla' p = \nabla P/P_c - \rho_0 L_c g/P_c$. The dimensionless density is defined by $\rho' = (\rho - \rho_0)/\rho_c$, where $\rho_c = P_c/L_c g$. The introduction of the set of scaled variables $\{\tau = t/t_c, (x, z) = (X, Z - L_z/2)/L_c, (a, b, c) = (A, B, C)/B_0, \mathbf{v} = \mathbf{V}/V_c$ with $\mathbf{v} = (u, v)^T, p = P/P_c\}$ and dropping the primes to the dimensionless pressure gradient and dimensionless density leads to the following dimensionless equations:

$$\partial_\tau a + (\mathbf{v} \cdot \nabla) a = \delta_a \nabla^2 a - ab, \quad (7)$$

$$\partial_\tau b + (\mathbf{v} \cdot \nabla) b = \nabla^2 b - ab, \quad (8)$$

$$\partial_\tau c + (\mathbf{v} \cdot \nabla) c = \delta_c \nabla^2 c + ab, \quad (9)$$

$$\nabla p = \nabla^2 \mathbf{v} - (R_a a + R_b b + R_c c) \mathbf{1}_z, \quad (10)$$

$$\nabla \cdot \mathbf{v} = 0, \quad (11)$$

where $\delta_a = D_A/D_B$ and $\delta_c = D_C/D_B$ are the ratios between the molecular diffusion coefficients of the base and salt, respectively, to that of the acid. Following previous works²⁷ (also see Table II), we use $\delta_a = 0.64$ and $\delta_c = 0.48$. The solutal Rayleigh number R_i of species I, defined as

$$R_i = \frac{g B_0 L_c^3 \alpha_I}{D_B \nu}, \quad (12)$$

controls the solutal buoyancy contribution of each chemical species I to the convective flows. In Eq. (12), $\nu = \mu/\rho_0$ is the kinematic viscosity of the medium. Defining the vorticity $\omega = \nabla \times \mathbf{v}$ and the stream function, ψ , through the relations, $u = \partial_z \psi$, $v = -\partial_x \psi$, the equations can be written in the $(\omega - \psi)$ form by taking the curl of both sides of Eq. (10). Our RDC model then reads

$$\frac{\partial a}{\partial \tau} + \left(\frac{\partial \psi}{\partial z} \frac{\partial c}{\partial x} - \frac{\partial \psi}{\partial x} \frac{\partial c}{\partial z} \right) = \delta_a \nabla^2 a - ab, \quad (13)$$

$$\frac{\partial b}{\partial \tau} + \left(\frac{\partial \psi}{\partial z} \frac{\partial c}{\partial x} - \frac{\partial \psi}{\partial x} \frac{\partial c}{\partial z} \right) = \nabla^2 b - ab, \quad (14)$$

$$\frac{\partial c}{\partial \tau} + \left(\frac{\partial \psi}{\partial z} \frac{\partial c}{\partial x} - \frac{\partial \psi}{\partial x} \frac{\partial c}{\partial z} \right) = \delta_c \nabla^2 c + ab, \quad (15)$$

$$\nabla^2 \omega = R_b \left[\frac{R_a}{R_b} \frac{\partial a}{\partial x} + \frac{\partial b}{\partial x} + \frac{R_c}{R_b} \frac{\partial c}{\partial x} \right], \quad (16)$$

$$\frac{\partial^2 \psi}{\partial x^2} + \frac{\partial^2 \psi}{\partial z^2} = -\omega. \quad (17)$$

TABLE II. Values for the parameters in Eqs. (13)–(17).

(I) Species	D_I (10^{-5} cm ² /s)	α_I (10 cm ³ /mol)	δ_i	α_I/α_B
(A) NaOH	2.129	4.4	0.64	2.5
(B) HCl	3.336	1.8	1.00	1.0
(C) NaCl	1.611	4.1	0.48	2.3

Given the uncertainty about the reaction rate constant k , which is embedded in L_c in the definition of the Rayleigh number, we cannot aim at a quantitative estimation of the parameters from experimental data. Nevertheless, we can obtain reliable re-scaled pictures of the problem by setting $R_b = 1$ and computing the ratios R_a/R_b as equal to α_a/α_b and $R_c/R_b = \alpha_c/\alpha_b$. In this way, the amplitude of the stream function remains arbitrary but the dynamics induced by the relative weight of each species to the density profile is kept balanced, since the proper ratios α_A/α_B and α_C/α_B are preserved. According to the results reported in Almarcha *et al.*,²⁷ we set $R_a/R_b = 2.5$ and $R_c/R_b = 2.3$ (see Table II).

B. Numerical scheme

The systems (13)–(17) are solved by using the alternating direction implicit method (ADI) proposed by Peaceman and Rachford.⁴³ An iterative procedure ensures the convergence of ω and ψ over the entire spatial domain at any time step, requiring the error between the stream function at the $(n - 1)$ th and (n) th iterations to be lower than 1×10^{-5} .

We consider a spatial domain of dimensionless width $L_x = 250$ and height $L_z = 400$, discretized over a grid of 500×800 points, by using equal horizontal and vertical meshes $hx = hz = 0.5$.

We apply no-flux boundary conditions for the concentration fields i of species I at the four solid boundaries of the reactor. No-slip conditions at the rigid walls directly apply to the stream function as

$$\psi = \frac{\partial \psi}{\partial x} = 0 \quad \text{at } x = 0; \quad x = L_x, \quad (18)$$

$$\psi = \frac{\partial \psi}{\partial z} = 0 \quad \text{at } z = 0; \quad z = L_z. \quad (19)$$

From the no-slip boundary conditions, a second order form for the rigid wall vorticity can be derived according to Woods' formula,⁴⁴

$$\omega|_x = -\frac{3 \psi|_{x+hx}}{(hx)^2} - \frac{1}{2} \omega|_{x+hx} \quad \text{at } x = 0, \quad (20)$$

$$\omega|_x = -\frac{3 \psi|_{L_x-hx}}{(hx)^2} - \frac{1}{2} \omega|_{L_x-hx} \quad \text{at } x = L_x, \quad (21)$$

$$\omega|_z = -\frac{3 \psi|_{z+hz}}{(hz)^2} - \frac{1}{2} \omega|_{z+hz} \quad \text{at } z = 0, \quad (22)$$

$$\omega|_z = -\frac{3 \psi|_{L_z-hz}}{(hz)^2} - \frac{1}{2} \omega|_{L_z-hz} \quad \text{at } z = L_z. \quad (23)$$

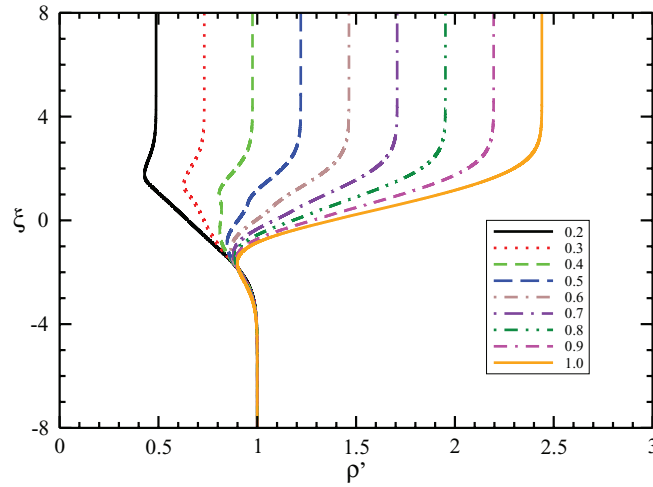


FIG. 8. Asymptotic dimensionless density profiles $\rho'(a, b, c)$ as a function of the re-scaled variable ξ for different ratios a_0/b_0 of initial concentrations, with $b_0 = 1$ mol/l. The initial contact line is at $\xi = 0$.

Simulations are run for 300 time units, using the time step $ht = 1 \times 10^{-3}$, which was tested to give convergent solutions. The step functions defining the initial distribution of the reactants,

$$a_0(x, z) = \begin{cases} [0.38, 0.42] & \text{if } z \geq L_z/2 \\ 0 & \text{elsewhere} \end{cases},$$

$$b_0(x, z) = \begin{cases} 1 & \text{if } z \leq L_z/2 \\ 0 & \text{elsewhere} \end{cases},$$

are added of a small amount of numerical noise at the interface in order to favour the emergence of the instability and speed up calculations. The stability and reliability of the numerical code were validated by recovering the results previously obtained for similar systems.³¹

C. Density profiles

A first theoretical approach consists in analyzing the asymptotic dimensionless density profiles $\rho'(a, b, c, \xi)$.²⁷ These are derived by introducing in the explicit relation,

$$\rho'(a, b, c, \xi) = \frac{R_a}{R_b} a(\xi) + b(\xi) + \frac{R_c}{R_b} c(\xi), \quad (24)$$

the numerical asymptotic solutions to the pure reaction-diffusion problem (13)–(15), with $\psi = 0$. At long times ($\tau \rightarrow \infty$), a balance occurs between reaction and diffusion rates, which gives rise to asymptotic concentration profiles in the re-scaled variable $\xi = z/\sqrt{\tau}$. The resulting density profiles for different initial concentrations a_0 are plotted in the vertical orientation to facilitate the comparison with our experimental geometry (see Fig. 8). The density of the pure solution B (A) is recovered as $\xi \rightarrow -\infty$ ($+\infty$). For example, if we consider the case where the initial concentration of A is $a = a_0/b_0 = 0.2$, as $\xi \rightarrow +\infty$ Eq. (24) reduces to $\rho'(a, b, c, +\infty) = \frac{R_a}{R_b} a = 0.5$, since the concentrations of b and c tend here to zero. In virtue of analogous considerations, the bottom density is equal to the constant value $\rho'(a, b, c, -\infty) = b = 1$. Approaching the interface ($\xi \rightarrow 0^\pm$), all the species contribute to the nonmonotonic configuration of the dimensionless density. Although $\rho'(a, b, c, \xi)$ do not contain any dynamic information on the system since they do not take into account the coupling with convective flows, they provide qualitative insights on the instability scenarios to be expected and, indeed, can give key elements to explain the experimental outcomes.

Let us first describe the curves corresponding to the alkaline concentration interval [0.2–0.4]. The top solution is less dense than the bottom one, which means that the initial stratification is

statically stable. However, as the solute in the lower denser solution (HCl) diffuses faster than the one in the upper solution (NaOH), the system is unstable with regard to a double-diffusive mechanism. In addition, because of the chemical reaction, the density profile is nonmonotonic as a minimum appears above the initial contact line. This is due to the formation of less concentrated NaCl, which moves upwards towards the less concentrated solution and replaces the reactants.^{31,33} The presence of this minimum implies that a denser solution locally overlies a less dense one. This region is buoyantly unstable and convection is likely to develop here. This situation corresponds to the experiments where convection appears *embedded* in the top of the system. Moreover, it has been observed throughout the experiments that the system becomes more unstable as the concentration of NaOH increases. This is also consistent with the description provided by asymptotic density profiles. It has indeed been shown that the strength of convection induced by extrema in a density profile can be related to the relative magnitude of these extrema with respect to the magnitude of the density jump between the two reactants.²⁶ Here, as the initial concentration of NaOH in the upper layer increases, the density jump between the two reactants decreases, while the magnitude of the minimum increases. In other words, the stable feature is diminished, while the unstable feature increases. This trend can be related to the experimental data plotted in Fig. 6, where the finger growth, and thus the hydrodynamic instability, develop faster as the top solution concentration approaches the threshold concentration 0.4.

If we now focus on the domain of the Rayleigh-Taylor instability (profiles in the range [0.5–1]), the system is globally RT unstable, as the top solution is denser than the lower one. However, due to the chemical reaction, a minimum appears in the reaction zone. This minimum can be considered as a stabilizing barrier that prevents the convective patterns from developing downwards, and leads to a breaking of the symmetry of the resulting Rayleigh-Taylor pattern.²⁶ It must be noted that at larger NaOH concentrations the pattern recovers the classical RT symmetry. Indeed, the system becomes readily unstable as the characteristic hydrodynamic time is then shorter than the time scale related to the chemical reaction. As a consequence, the stabilizing minimum in density does not have time to develop. A genuine example of this fact is the symmetric dynamics exhibited by the system when the concentration of the upper alkaline solution is 1 (solid curves in Fig. 5(b)).

D. Nonlinear simulations

A further confirmation of the dramatic influence of chemical processes in the symmetry of hydrodynamic instabilities can be obtained by means of numerical simulations of the nonlinear RDC systems (13)–(17). Following the experimental approach, we explore here spatio-temporal scenarios observed in the transition from a DD regime to the RT instability by varying the initial jump of density ($\rho_A^0 - \rho_B^0$) between the two solutions. The initial concentration a_0 is taken in the range [0.38–0.42] with $R_a/R_b = 2.5$, keeping the concentration of the bottom solution $b_0 = 1$ constant, which corresponds to scan the dimensionless density $\rho' = R_a/R_b a_0$ of the upper solution in the interval [0.98–1.02] over a solution with unitary density (see Fig. 7, right panel). Within this density range, the transition from the DD to the RT regime is smooth, as the density jump is small and the effect played by the chemical reaction is large. As discussed in Sec. III C, if the density jump between the two solutions is too large, the global dynamics then falls back into the traditional non reactive hydrodynamic scenarios. We directly compare the spatio-temporal evolution of the concentration fields in the reactive cases to the analogous non reactive scenarios obtained by neglecting kinetic terms in Eqs. (13)–(15). A consistent comparison is made by using the same general conditions and parameters ($R_a = 2.5$, $\delta_a = 0.64$) both in the non reactive and reactive cases, the latter ones also considering the parameters for the species C, $R_c = 2.3$, and $\delta_c = 0.48$.

We compute the temporal evolution of the two separate contributions to the total mixing length, $L_m^+ = z_{top} - z_0$ and $L_m^- = z_{bottom} - z_0$, whose magnitude gives the entity of the upward and downward finger growth referred to the initial contact line at $z_0 = L_z/2$. The definition of L_m^+ and L_m^- is based, in the numerics, on the transversely averaged value of the concentration profile $a(x, z, t)$ over the x -direction, at a given time t :⁴⁵

$$\langle a \rangle(z, t) = \frac{1}{L_x} \int_0^{L_x} a(x, z, t) dx, \quad (25)$$

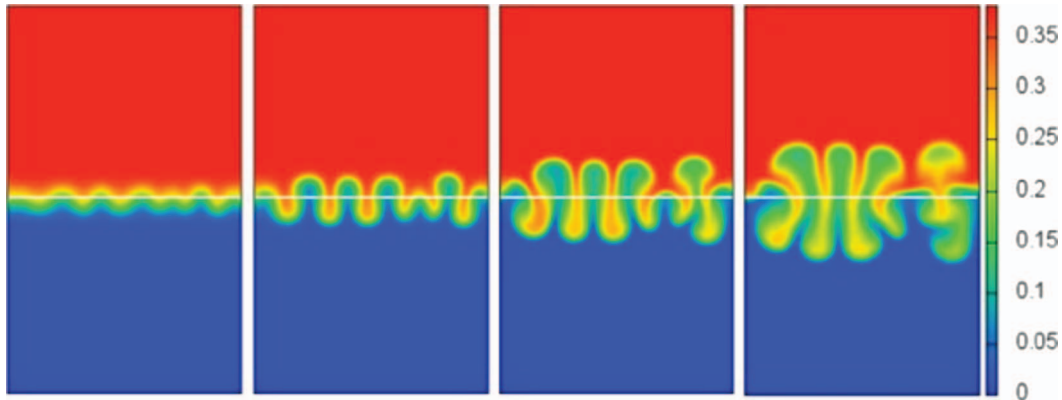


FIG. 9. Numerical non reactive double-diffusive pattern when the top solution A is less dense ($\rho_1 = 0.98$, $a_0/b_0 = 0.38$, $R_a = 2.5$) than the underlying solution B, and solute B diffuses faster than A ($\delta_a = 0.64$). The numerical concentration map for species A is reported at times 130, 180, 220, and 260. The size of the spatial domain is $L_x = 250 \times L_z = 400$ and the aspect ratio is preserved.

and, typically, $z_{top} = \sup\{z : \langle a \rangle(z, t) \leq 0.99\}$ and $z_{bottom} = \sup\{z : \langle a \rangle(z, t) \leq 0.01\}$. The mixing length is computed with regard to the concentration of A, since it diffuses slower and provides steeper concentration gradients for the identification of edge points. Time series for L_m^+ and L_m^- is built up by collecting z_{top} and z_{bottom} as functions of time.

1. Double diffusion

We first consider the DD case starting from the initial density profile ρ_1 shown in Fig. 7, right panel. Figure 9 illustrates the emergence of fingers in the absence of any reactive process. Here, the dynamics is followed by showing the concentration of species A. The distribution of B is similar (though more blurry as this species diffuses here faster) and hence not shown. Note that, although the experimental figures show refractive index fields, the dynamics of the concentration fields computed numerically are similar, as the refractive index of the solution is related to its composition. In the fully developed nonlinear regime, the finger growth is characterized by a symmetry with regard to the initial position of the interface between the two reactants, represented as a white line in each snapshot. The origin of this symmetry is intrinsic in the particular form of the equations and the base-state profiles of the initial concentration, and is extensively discussed by Trevelyan *et al.*²

As found in the experimental results, this symmetry is broken by the chemical reaction as illustrated in Fig. 10. The instability develops on a time scale comparable with the non reactive case, nevertheless, the fingers exhibit a preferential growth in the upward direction. The breaking of

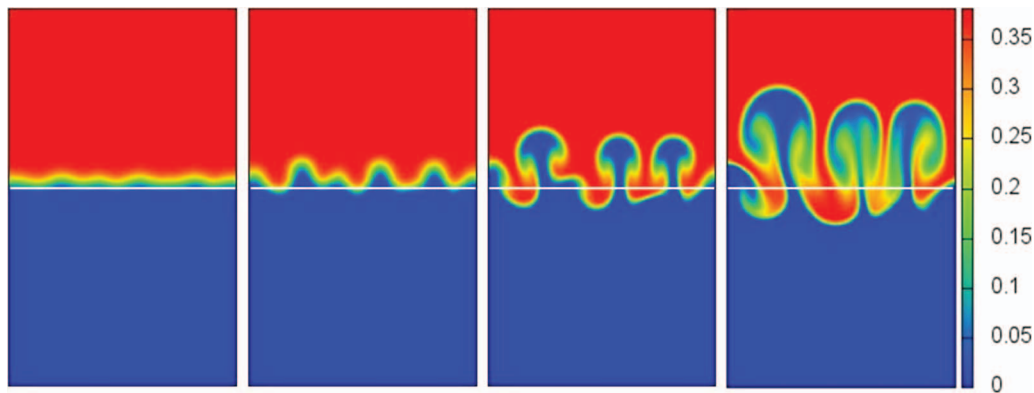


FIG. 10. Asymmetric reactive double-diffusive pattern affected by the reaction $A + B \rightarrow C$ ($\delta_c = 0.48$, $R_c = 2.3$). All other conditions are the same as in Fig. 9.

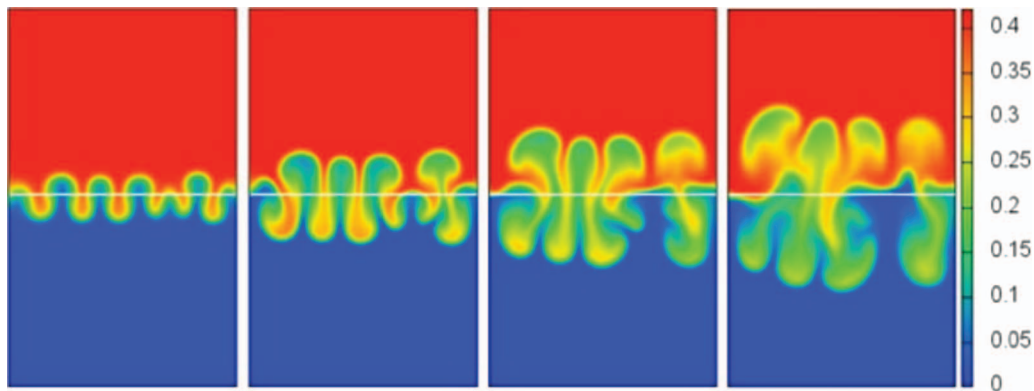


FIG. 11. Symmetric non reactive Rayleigh-Taylor pattern. All conditions are the same as in Fig. 9 except that the top solution A is now denser ($\rho_2 = 1.02$, $a_0/b_0 = 0.42$) than the underlying solution B.

symmetry, favored by the formation of the salt according to the mechanism discussed in Sec. III C, is quantitatively followed in Fig. 13(a) comparing the evolution of the mixing lengths L_m^+ and L_m^- for the reactive (squares) and non reactive (triangles) cases. The curves described by triangles are consistent with a standard behavior due to a DD mechanism. After an initial period (~ 200 time units) driven by the diffusive process in which $L_m^{+/-}$ scale as \sqrt{t} , the system switches to a convective linear growth $L_m^{+/-} \sim vt$. The mirror behavior delineated by L_m^+ and L_m^- is clearly not preserved when the interface dynamics is affected by the chemical reaction. In the reactive case, L_m^+ initially follows that of the non reactive case, but diverges from it as soon as the system is controlled by the convective instability. On the other hand, L_m^- , negligible during the diffusive regime, only slowly diverges from the initial reference position. The patterns obtained by numerical simulations closely remind those found in the experiments.

2. Rayleigh-Taylor

When the starting concentration of solution A, a_0 , is increased beyond the threshold 0.4, the upper layer of the system becomes denser than the bottom solution (see the profile ρ_2 in Fig. 7, right panel) and the resulting dynamics undergoes a RT instability. The onset and the development of the density fingering are followed in Fig. 11. The distortion of the planar interface between the two fluids is symmetric with respect to the initial contact line.

Here again, in the reactive case, the denser solute A is consumed to produce C of intermediate density which, in turn, suppresses the finger formation along the downward direction (see Sec. III C) as seen in Fig. 12. The peculiar asymmetry is highlighted by comparing the concentration map of A

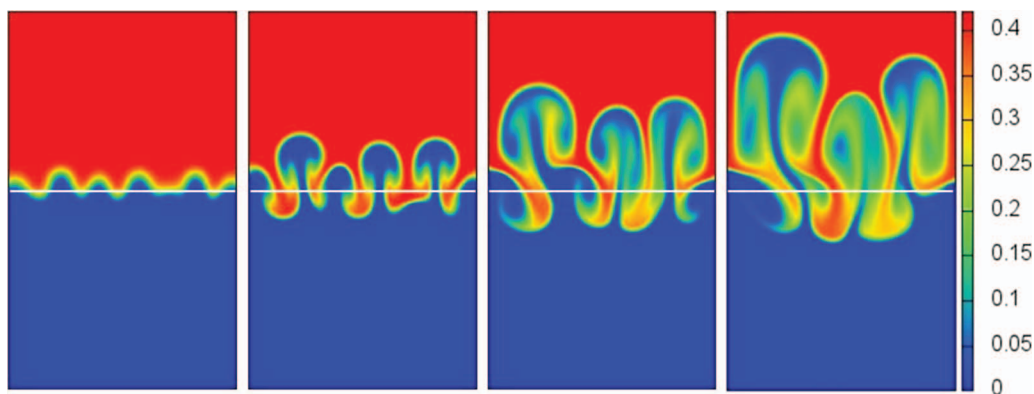


FIG. 12. Asymmetric reactive Rayleigh-Taylor affected by the reaction $A + B \rightarrow C$ ($\delta_c = 0.48$, $R_c = 2.3$). The same conditions as in Fig. 11 are considered.

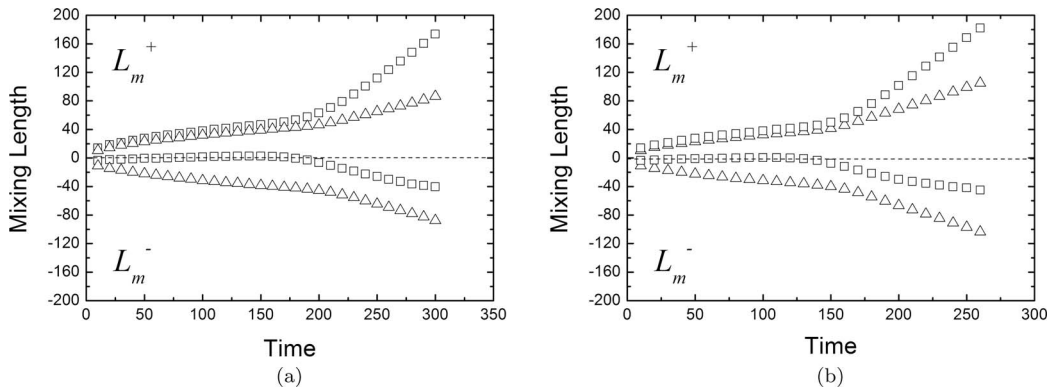


FIG. 13. Upward (L_m^+) and downward (L_m^-) contribution to the total mixing length as a function of time for the (a) double-diffusive and (b) Rayleigh-Taylor scenarios. Triangles trace the mixing length dynamics related to the pure hydrodynamic instability, while squares follow the reactive case.

at the same times as in Fig. 11 and by tracing the dynamics of L_m^+ and L_m^- as a function of time in Fig. 13(b). Once more, the simulations are in agreement with the related experimental findings.

The parallel between Figs. 9–12 points out the strong similarity exhibited in the spatio-temporal patterns of the RT or DD instability, both in the presence or absence of the chemical contribution. This feature has already been discussed in a previous paper by Trevelyan *et al.*² and was found to be correlated to the similar topology of the ψ eigenfunctions in proximity of the interface, where the instability actually develops. Physically this means that the density profiles at the basis of the hydrodynamic flow present similar symmetries with a local minimum located at almost the same position along the vertical direction, close to the initial interface. For the small initial density jump considered here, the transition from the DD to the RT scenarios is smooth. Hence, the system can be destabilized by an analogous wavelength, while different modes can be observed by further increasing the density difference between the two layers. However, the RT instability develops faster than the DD one as seen by comparing Figs. 13(a) and 13(b), since a longer time is needed for DD to set in.

IV. CONCLUSIONS

We have analyzed, both experimentally and theoretically, the influence that a simple $A + B \rightarrow C$ reaction can have on convective Rayleigh-Taylor and double-diffusive modes at the interface of a solution of A overlying another miscible solution of B of different density in the gravitational field. We have shown that the chemical reaction breaks the symmetry of the convective patterns in the sense that the resulting fingers extend preferentially above the initial contact line for the acid/base reaction chosen here, while they develop symmetrically around it in the non reactive case. This is related to the fact that species A and B are consumed in the course of time to yield the product C of different density.

We observe that, in the RT convective regime, the influence of the chemical reaction on the pattern evolution loses importance when the endpoint density contrast increases. In other words, the symmetry of the convective RT pattern is recovered when the upper solution is sufficiently denser than the lower one for the chemical reaction to be ineffective to modify the RT instability. Further quantitative studies to delineate the exact conditions for chemistry to be operative remain to be developed.

Finally, we have also observed experimentally that within the reactive double diffusion regime, a second striped pattern can develop later below the first fingered pattern. This second pattern can be attributed to a secondary double diffusive instability between the slow diffusing reaction product (NaCl) and the fast diffusing bottom reactant (HCl).

These results point to the importance of taking chemical reactions into account in any modeling of reactive fluid flow processes. If the reaction actively modifies a physical property of the fluid like the density here, one cannot avoid taking the kinetics of the processes into account in the analysis of the problem as clearly the symmetries of the pattern which develop and their nonlinear dynamics are different than in the non reactive case. The understanding of this paves the way to a wealth of new experimental and theoretical studies that should focus on deciphering the active role of chemical reactions in the numerous applications in which Rayleigh-Taylor and double diffusion instabilities are observed.

ACKNOWLEDGMENTS

Help from F. Haudin in the analysis of the experimental results is gratefully acknowledged. We also thank P. M. J. Trevelyan and C. Almarcha for fruitful discussions. A.D. acknowledges financial support from the Fonds National de la Recherche Scientifique (FRS-FNRS, Belgium) and Prodex. P.G. thanks FRS-FNRS for financial support under contract C-Net NR/FVH972. L.R. is a Marie-Curie EU-FP7/ITN Multiflow fellow, while L.L. and M.B. are both Prodex fellows. All these sources of funding are gratefully acknowledged.

- ¹ S. Chandrasekhar, *Hydrodynamic and Hydromagnetic Stability* (Dover, New York, 1981); P. G. Drazin and W. H. Reid, *Hydrodynamic Stability* (Cambridge University Press, Cambridge, 2004).
- ² P. M. J. Trevelyan, C. Almarcha, and A. De Wit, "Buoyancy-driven instabilities of miscible two-layer stratifications in porous media and Hele-Shaw cells," *J. Fluid Mech.* **670**, 38 (2011).
- ³ J. Fernandez, P. Kurowski, P. Petitjeans, and E. Meiburg, "Density-driven unstable flows of miscible fluids in a Hele-Shaw cell," *J. Fluid Mech.* **451**, 239 (2002).
- ⁴ J. S. Turner, *Buoyancy Effects in Fluids* (Cambridge University Press, Cambridge, 1979).
- ⁵ H. E. Huppert and J. S. Turner, "Double-diffusive convection," *J. Fluid Mech.* **106**, 299 (1981).
- ⁶ C. A. Cooper, R. J. Glass, and S. W. Tyler, "Experimental investigation of the stability boundary for double-diffusive finger convection in a Hele-Shaw cell," *Water Resour. Res.* **33**, 517, doi:10.1029/96WR03811 (1997).
- ⁷ S. E. Pringle and R. J. Glass, "Double-diffusive finger convection: Influence of concentration at fixed buoyancy ratio," *J. Fluid Mech.* **462**, 161 (2002).
- ⁸ R. W. Schmitt, "Double diffusion in oceanography," *Annu. Rev. Fluid Mech.* **26**, 255 (1994).
- ⁹ O. P. Singh, D. Ranjan, J. Srinivasan, and K. R. Sreenivas, "A study of basalt fingers using experiments and numerical simulations in double-diffusive systems," *J. Geogr. Geol.* **3**, 42 (2011).
- ¹⁰ C. Wylock, S. Dehaeck, A. Rednikov, and P. Colinet, "Chemo-hydrodynamical instability created by CO₂ absorption in an aqueous solution of NaHCO₃ and Na₂CO₃," *Microgravity Sci. Technol.* **20**, 171 (2008).
- ¹¹ J. T. H. Andres and S. S. S. Cardoso, "Onset of convection in a porous medium in the presence of chemical reaction," *Phys. Rev. E* **83**, 046312 (2011).
- ¹² M. Chertkov, V. Lebedev, and N. Vladimirovna, "Reactive Rayleigh-Taylor turbulence," *J. Fluid Mech.* **633**, 1 (2009).
- ¹³ O. Citri, M. L. Kagan, R. Kosloff, and D. Avnir, "Evolution of chemically induced unstable density gradients near horizontal reactive interfaces," *Langmuir* **6**, 559 (1990).
- ¹⁴ A. De Wit, K. Eckert, and S. Kalliadasis, "Introduction to the Focus issue: Chemo-hydrodynamic patterns and instabilities," *Chaos* **22**, 037101 (2012).
- ¹⁵ L. A. Riolfo, Y. Nagatsu, S. Iwata, R. Maes, P. M. J. Trevelyan, and A. De Wit, "Experimental evidence of reaction-driven miscible viscous fingering," *Phys. Rev. E* **85**, 015304(R) (2012).
- ¹⁶ J. D'Hernoncourt, A. De Wit, and A. Zebib, "Double-diffusive instabilities of autocatalytic chemical fronts," *J. Fluid Mech.* **576**, 445 (2007).
- ¹⁷ L. Rongy, G. Schuszter, Z. Sinkó, T. Tóth, D. Horváth, A. Tóth, and A. De Wit, "Influence of thermal effects on buoyancy-driven convection around autocatalytic chemical fronts propagating horizontally," *Chaos* **19**, 023110 (2009).
- ¹⁸ J. D'Hernoncourt and A. De Wit, "Influence of heat losses on nonlinear fingering dynamics of exothermic autocatalytic fronts," *Physica D* **239**, 819 (2010).
- ¹⁹ L. Biferale, F. Mantovani, M. Sbraglia, A. Scagliarini, F. Toschi, and R. Tripiccion, "Reactive Rayleigh-Taylor systems: Front propagation and non-stationarity," *Europhys. Lett.* **94**, 54004 (2011).
- ²⁰ K. Eckert and A. Grahn, "Plume and finger regimes driven by an exothermic interfacial reaction," *Phys. Rev. Lett.* **82**, 4436 (1999).
- ²¹ K. Eckert, M. Acker, and Y. Shi, "Chemical pattern formation driven by a neutralization reaction. I. Mechanism and basic features," *Phys. Fluids* **16**, 385 (2004).
- ²² A. Zalts, C. El Hasi, D. Rubio, A. Ureña, and A. D'Onofrio, "Pattern formation driven by an acid-base neutralization reaction in aqueous media in a gravitational field," *Phys. Rev. E* **77**, 015304(R) (2008).
- ²³ K. Tanoue, H. Ikemoto, M. Yoshitomi, and T. Nishimura, "Instabilized heat and mass transfer in exothermic chemically reacting flows," *Therm. Sci. Eng.* **17**, 121 (2009).
- ²⁴ C. Almarcha, P. M. J. Trevelyan, P. Grosfils, and A. De Wit, "Chemically driven hydrodynamic instabilities," *Phys. Rev. Lett.* **104**, 044501 (2010).

- ²⁵ C. Almarcha, P. M. J. Trevelyan, L. A. Riolfo, A. Zalts, C. El Hasi, A. D'Onofrio, and A. De Wit, "Active role of a color indicator in buoyancy-driven instabilities of chemical fronts," *J. Phys. Chem. Lett.* **1**, 752 (2010).
- ²⁶ S. Kuster, L. A. Riolfo, A. Zalts, C. El Hasi, C. Almarcha, P. M. J. Trevelyan, A. De Wit, and A. D'Onofrio, "Differential diffusion effects on buoyancy-driven instabilities of acid-base fronts: The case of a color indicator," *Phys. Chem. Chem. Phys.* **13**, 17295 (2011).
- ²⁷ C. Almarcha, Y. R'Honi, Y. De Decker, P. M. J. Trevelyan, K. Eckert, and A. De Wit, "Convective mixing induced by acid-base reactions," *J. Phys. Chem. B* **115**, 9739 (2011).
- ²⁸ K. Tsuji and S. C. Müller, "Chemical reaction evolving on a droplet," *J. Phys. Chem. Lett.* **3**, 977 (2012).
- ²⁹ K. Eckert, L. Rongy, and A. De Wit, "A + B → C reaction fronts in Hele-Shaw cells under modulated gravitational acceleration," *Phys. Chem. Chem. Phys.* **14**, 7337 (2012).
- ³⁰ L. Rongy, P. M. J. Trevelyan, and A. De Wit, "Dynamics of A + B → C reaction fronts in the presence of buoyancy-driven convection," *Phys. Rev. Lett.* **101**, 084503 (2008).
- ³¹ L. Rongy, P. M. J. Trevelyan, and A. De Wit, "Influence of buoyancy-driven convection on the dynamics of A + B → C in reaction fronts in horizontal solution layers," *Chem. Eng. Sci.* **65**, 2382 (2010).
- ³² S. H. Hejazi and J. Azaiez, "Stability of reactive interfaces in saturated porous media under gravity in the presence of transverse flows," *J. Fluid Mech.* **695**, 439 (2012).
- ³³ L. Gálfi and Z. Ràcz, "Properties of the reaction front in an A + B → C type reaction-diffusion process," *Phys. Rev. A* **38**, 3151 (1988).
- ³⁴ R. W. Griffiths, "Layered double-diffusive convection in porous media," *J. Fluid Mech.* **102**, 221 (1981).
- ³⁵ M. S. Malashetty and S. N. Gaikwad, "Onset of convective instabilities in a binary liquid mixtures with fast chemical reactions in a porous medium," *Heat Mass Transfer* **39**, 415 (2003).
- ³⁶ M. S. Malashetty and B. S. Biradar, "The onset of double diffusive reaction-convection in an anisotropic porous layer," *Phys. Fluids* **23**, 064102 (2011).
- ³⁷ D. Pritchard and C. N. Richardson, "The effect of temperature-dependent solubility on the onset of thermosolutal convection in a horizontal porous layer," *J. Fluid Mech.* **571**, 59 (2007).
- ³⁸ Y. Shi and K. Eckert, "A novel Hele-Shaw cell design for the analysis of hydrodynamic instabilities in liquid-liquid systems," *Chem. Eng. Sci.* **63**, 3560 (2008).
- ³⁹ G. S. Settles, *Schlieren and Shadowgraph Techniques* (Springer, Berlin, 2001).
- ⁴⁰ L. Joannes, F. Dubois, and J.-C. Legros, "Phase-shifting schlieren: High-resolution quantitative schlieren that uses the phase-shifting technique principle," *Appl. Opt.* **42**, 5046 (2003).
- ⁴¹ W. M. Haynes, *CRC Handbook of Chemistry and Physics*, 92nd ed. (CRC, Boca Raton, 2011).
- ⁴² R. C. Weast, *CRC Handbook of Chemistry and Physics*, 56th ed. (CRC, Cleveland, 1975).
- ⁴³ D. W. Peaceman and H. H. Rachford, "The numerical solution of parabolic and elliptic differential equations," *J. Soc. Ind. Appl. Math.* **3**, 28 (1955).
- ⁴⁴ L. C. Woods, "A note on the numerical solution of fourth order differential equations," *Aeronaut. Q.* **5**, 176 (1954).
- ⁴⁵ A. De Wit, "Miscible density fingering of chemical fronts in porous media: Nonlinear simulations," *Phys. Fluids* **16**, 163 (2004).